

Are β -H Eliminations or Alkene Insertions Feasible Elementary Steps in Catalytic Cycles Involving Gold(I) Alkyl Species or Gold(I) Hydrides?

Günter Klatt,^[a] Rong Xu,^[a] Markus Pernpointner,^[a] Lise Molinari,^[b]
Tran Quang Hung,^[b] Frank Rominger,^[b] A. Stephen K. Hashmi,^[b] and Horst Köppel*^[a]

Abstract: The β -H-elimination in the (iPr)AuEt complex and its microscopic reverse, the insertion of ethene into (iPr)AuH, were investigated in a combined experimental and computational study. Our DFT-D3 calculations predict free-energy barriers of 49.7 and 36.4 kcal mol⁻¹ for the elimination and insertion process, respectively, which permit an estimation of the rate constants for these reactions according to classical transition-state theory. The elimination/insertion pathway is found to involve a high-energy ethene hydride species and is not significantly af-

ected by continuum solvent effects. The high barriers found in the theoretical study were then confirmed experimentally by measuring decomposition temperatures for several different (iPr)Au^I-alkyl complexes which, with a slow decomposition at 180 °C, are significantly higher than those of other transition-metal alkyl complexes. In addition, at the same temperature, the

decomposition of (iPr)AuPh and (iPr)AuMe, both of which cannot undergo β -H-elimination, indicates that the pathway for the observed decomposition at 180 °C is not a β -H-elimination. According to the calculations, the latter should not occur at temperatures below 200 °C. The microscopic reverse of the β -H-elimination, the insertion of ethene into the (iPr)AuH could neither be observed at pressures up to 8 bar at RT nor at 1 bar at 80 °C. The same is true for the strain-activated norbornene.

Keywords: alkenes • computational chemistry • elimination • gold • hydrides • insertion

Introduction

For a long time gold hydride complexes were assumed to have a low stability.^[1] This was supposed to be the reason for not observing β -H-eliminations in homogeneous gold catalysis,^[2,3] whereas these reactions are commonplace in catalysts of other transition metals. They often constitute elementary steps in many catalytic processes, for example, the isomerization of higher alkyls to metal hydrides. The inverse reaction, ethene insertion into a metal–hydrogen bond, is analogous to the rate-determining insertion step of transition-metal-catalyzed olefin polymerization.^[4] The results obtained in gold-catalyzed reactions^[5] clearly indicate a lack of β -H-elimination, but the recent isolation of a NHC-gold(I)

monohydride^[6] and a dinuclear gold(I) hydride^[7] in a spectacular manner disprove a general low stability of gold hydride complexes.

The reactivity of NHC-gold(I) monohydride with regard to typical elementary steps of catalysis reactions has been investigated;^[6] normal alkynes such as 1-hexyne and diphenylacetylene do not insert into the gold–hydrogen bond, but dimethyl acetylenedicarboxylate does. Unexpectedly, for the insertion product a crystal structure analysis showed an *anti*-arrangement of the NHC-gold fragment and the hydride, which excludes a concerted *syn*-insertion pathway (the microscopic reverse of a β -H-elimination). On the other hand, the investigation neither could rule out a radical mechanism nor a *syn*-addition/isomerization sequence. Previously, gold(III) monohydrides had already been suggested as intermediates in homogeneous gold-catalyzed hydrogenation reactions, a pathway that was supported by DFT calculations^[8] and an active participation of gold(I) hydrides in the dehydrogenative silylation of alcohols had been proposed (the reported hydrolysis of NHC-gold(I) monohydride would nicely fit into that picture).^[9] Another recent publication^[10] reports a gold(I) hydride species, which could be characterized by ¹H and ³¹P NMR spectroscopic measurements and ESI mass spectrometry. NMR and kinetic studies revealed that the reaction mechanism of the dehydrogenative silylation indeed involves the gold(I) hydride species as a key intermediate.

Lately, a report stressed a β -H-elimination as an elementary step in a gold(III)-catalyzed reaction forming strained

[a] Dr. G. Klatt, Dr. R. Xu, Dr. M. Pernpointner, Prof. Dr. H. Köppel
Physikalisch-Chemisches Institut
Ruprecht-Karls-Universität Heidelberg
Im Neuenheimer Feld 229
69120 Heidelberg (Germany)
Fax: (+49) 6221-545-221
E-mail: Horst.Koepfel@pci.uni-heidelberg.de

[b] L. Molinari, T. Quang Hung, Dr. F. Rominger,⁺
Prof. Dr. A. S. K. Hashmi
Organisch-Chemisches Institut
Ruprecht-Karls-Universität Heidelberg
Im Neuenheimer Feld 270
69120 Heidelberg (Germany)
Fax: (+49) 711-685-4205

[⁺] Crystallographic investigation

oxetenes.^[11] The claim is supported by calculations at the PCM(CH₂Cl₂)-B3LYP/def2-SVP level.

Since this elemental step could be of significant importance for developing new catalytic cycles in homogeneous gold catalysis, we now decided to conduct a detailed investigation of the β -H-elimination (respectively its microscopic reverse, the alkene insertion pathway which is of importance for gold-catalyzed hydrogenations) for gold(I) as the most frequently used oxidation state in homogeneous gold catalysis.

Computational Details

We performed initial geometry optimizations at the B3LYP/cc-pVDZ level of theory for all calculated species using the Gaussian 09 software package.^[12] In this basis, the gold atom is described by the (8 s7p6d1f)/[4s4p3d1f] pseudopotential-based correlation consistent basis set of Peterson and Puzarini,^[13] and the light atoms by Dunning's cc-pVDZ basis functions.^[14] For gold a relativistic effective core potential (RECP) was employed,^[15] which replaced the innermost 60 electrons. This RECP was designed to accurately account for relativistic effects, such as s orbital contraction and d-orbital expansion, and has proven to be very successful for calculations of organometallic compounds.^[16] All stationary points involved were fully optimized. Frequency calculations were undertaken to confirm the nature of the stationary points, yielding one imaginary frequency for transition states (TS) and zero for minima. Transition states were obtained by either a combined scanning and transit-guided quasi-Newton (STQN) method, or a combination of the two STQN approaches LST^[17] and QST3,^[18] as implemented in Gaussian 09. The connectivity of the transition states and their adjacent minima was confirmed by intrinsic reaction coordinate (IRC) calculations. Zero-point energy (ZPE) corrections were carried out for all computed energies. Free energies G_{298} were calculated by using the harmonic approximation and standard textbook procedures. To obtain estimates on the solvent effect, we made use of the polarizable continuum model (PCM) method with the dielectric constant for dichloromethane to generate single-point energies at the B3LYP/cc-pVDZ-optimized geometries. These were then used in the calculation of ZPE-corrected energies E_0 and free energies G_{298} based on the B3LYP/cc-pVDZ harmonic frequencies.

Very recently, an implementation of Grimme's D3 dispersion parameters^[19] into the Turbomole 6.4 program^[20] has paved the way for calculations on large organometallic systems that include dispersive interactions; see for example reference [21]. To account for these forces, which are poorly described by standard DFT functionals, as well as to compare two different methods, we re-optimized all stationary points at the BP86-D3 level of theory, which contains Grimme's D3 dispersion parameters.^[19] The double ζ -quality basis set def2-SVP^[22] as well as the multipole-accelerated resolution of the identity approximation MARI-J with suitable fitting basis sets^[23] were used in these computations. Scalar relativistic effects were included by using a Stuttgart ECP for gold.^[24]

For the complexes [(*i*Pr)AuEt] and [(*i*Pr)AuH], we additionally performed MP2 single-point energy calculations at the B3LYP/cc-pVDZ-optimized geometries, that is, for the MP2/cc-pVDZ//B3LYP/cc-pVDZ model chemistry. ZPE-corrections and free energies were obtained in the same manner as for the PCM calculations.

Results and Discussion

Intermediates and transition states of the β -elimination pathway: Taking into account the importance of the *i*Pr ligand for the stabilization of gold(I) hydride, we decided to investigate the thermal decay of (*i*Pr)AuEt to form the re-

cently reported gold hydride complex (*i*Pr)AuH^[6] as well as free ethene. The starting points for our work were the X-ray crystal structures of the (*i*Pr)AuEt (which was determined in the course of this investigation)^[25] and (*i*Pr)AuH complexes (which had been determined previously).^[6] We subjected these structures to DFT geometry optimization and arrived at structures **1** and **2**, which are given in Figure 1 together with the atom numbering adopted in the following discussion, and for which selected structural parameters are displayed in Table 1.

The calculated bond lengths generally agree well (within 0.02 Å) with experiment, except for bonds involving either hydrogen atoms (which are difficult to pinpoint by X-ray crystallography) or the Au center, which is probably not as well described as the lighter atoms by the basis sets and methods used in this work. Notable exceptions are the C–C bond length in the ethyl group of **1**, which deviates by 0.05 Å (DFT: 1.54 Å, X-ray: 1.49 Å), and the C–C bond length in the NHC subunit, which deviates by 0.04 Å (DFT: 1.36 Å, X-ray: 1.32 Å).

Likewise, the angles obtained with our DFT methods also agree well (within 3–4°) with the experimental result, except for the larger deviations observed for several dihedrals, which is a likely consequence of their larger flexibility,

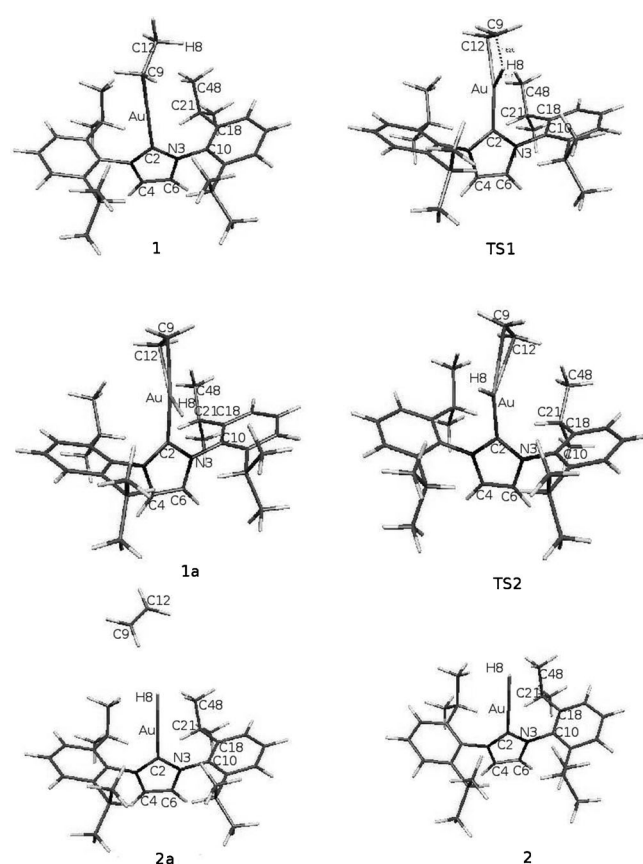


Figure 1. Stationary points of the thermal decay of (*i*Pr)AuEt. Compounds **1**, **1a**, **2a**, and **2** correspond to the ethyl complex, ethene hydride, van der Waals adduct and gold hydride plus free ethene, respectively. **TS1** and **TS2** represent the interconnecting transition states.

Table 1. Selected calculated and experimental bond lengths [Å] and angles [°] for stationary points of the thermal decay of (iPr)AuEt.^[a]

		1	TS1	1a	TS2	2a	2
Au-C9	Exp	2.133					∞
	BP86-D3/def2-SVP	2.086	2.289	2.143	2.348	4.025	∞
	B3LYP/cc-pVDZ	2.085	2.285	2.136	2.364	4.538	∞
Au-C12	Exp	3.030					∞
	BP86-D3/def2-SVP	3.055	2.280	2.209	2.462	4.819	∞
	B3LYP/cc-pVDZ	3.094	2.270	2.208	2.490	5.346	∞
H8-C9	Exp	0.980					∞
	BP86-D3/def2-SVP	1.112	1.613	3.133	2.900	3.626	∞
	B3LYP/cc-pVDZ	1.104	1.593	3.053	2.868	3.748	∞
Au-H8	Exp	3.128					1.750
	BP86-D3/def2-SVP	3.245	1.778	1.674	1.658	1.622	1.621
	B3LYP/cc-pVDZ	3.296	1.779	1.676	1.662	1.619	1.618
Au-C2	exp	1.999					1.999
	BP86-D3/def2-SVP	2.064	1.965	2.125	2.079	2.078	2.078
	B3LYP/cc-pVDZ	2.080	1.981	2.116	2.096	2.090	2.091
C2-N3	exp	1.373					1.357
	BP86-D3/def2-SVP	1.370	1.382	1.372	1.375	1.369	1.370
	B3LYP/cc-pVDZ	1.369	1.379	1.370	1.374	1.368	1.368
C9-C12	exp	1.489					
	BP86-D3/def2-SVP	1.542	1.453	1.439	1.390	1.342	
	B3LYP/cc-pVDZ	1.540	1.448	1.428	1.376	1.334	
C4-C6	exp	1.320					1.320
	BP86-D3/def2-SVP	1.372	1.369	1.371	1.370	1.371	1.371
	B3LYP/cc-pVDZ	1.359	1.355	1.355	1.357	1.359	1.359
C21-C48	exp	1.520					1.525
	BP86-D3/def2-SVP	1.541	1.542	1.543	1.538	1.541	1.544
	B3LYP/cc-pVDZ	1.540	1.539	1.538	1.538	1.541	1.540
Au-C2-N3	exp	127.6					130.3
	BP86-D3/def2-SVP	127.5	128.1	127.5	126.7	128.1	128.1
	B3LYP/cc-pVDZ	128.1	128.0	127.6	128.4	128.0	128.0
C10-C18-C21-C48	exp	150.0					151.3
	BP86-D3/def2-SVP	119.5	110.1	86.8	151.3	110.6	90.6
	B3LYP/cc-pVDZ	114.0	120.8	128.2	133.6	109.6	115.6
C2-N3-C10-C18	exp	-72.9					-88.0
	BP86-D3/def2-SVP	-80.6	-89.6	-98.2	-88.3	-84.0	-96.5
	B3LYP/cc-pVDZ	-90.2	-90.1	-90.7	-95.4	-90.9	-90.6

[a] Compounds **1**, **1a**, **2a**, and **2** correspond to the ethyl complex, ethene hydride, van der Waals adduct, and gold hydride plus free ethene, respectively. **TS1** and **TS2** represent the interconnecting transition states. Experimental data are available for structures **1** and **2** only. The atom numbering is given in Figure 1.

resulting in considerable crystal-packing effects in the solid state.

To determine a transition state for this reaction by using the LST-QST3 method, we reoptimized **2** after introduction of a free ethene molecule and obtained the van der Waals complex **2a**. It consists of the subunits (iPr)AuH and C₂H₄, for which the shortest distance is 2.660 Å, measured between the hydride and an ethene hydrogen atom (B3LYP/cc-pVDZ).

Our initial attempt to determine a transition state for the reaction **1**→**2a** by using the LST-QST3 method yielded a transition structure **TS1**, in which we found **1** to be connected to an ethylene-hydride isomer [(iPr)Au(C₂H₄)H] **1a**, in which both an ethene and a hydride ligand are connected to the metal center. The most striking feature of **1a** is an almost orthogonal arrangement of the NHC-Au-H structure with $\theta(\text{C2-Au-H}) = 96.8^\circ$ (B3LYP/cc-pVDZ). The Au-C bond lengths for the carbon atoms of the ethene ligand are 2.135 Å and 2.209 Å, respectively. The C-C distance in the

latter is 1.428 Å and thus substantially longer than the 1.333 Å calculated for free C₂H₄, which indicates the donation of electron density from the Au center into the antibonding π^* orbital.

TS1 corresponds to the breaking of the C-H bond in the methyl group and exhibits more structural similarity with **1a** than with the preceding alkyl structure **1**; in particular, the C-H distance has increased to 1.593 Å, indicating an already broken bond, whereas it remains below 1.3 Å in agostic transition-metal alkyls (see Table 2 in ref. [26]). The C-C bond has shortened to 1.448 Å, and the AuH bond length is 1.779 Å (B3LYP/cc-pVDZ).

We found **1a** to be connected to **2a** via the transition state **TS2**, as confirmed by IRC calculations. **TS2** is characterized by a C2-Au-H bond angle of 130.5° and a distance of 2.364 Å between Au and the nearest C atom of the ethene unit (B3LYP/cc-pVDZ).

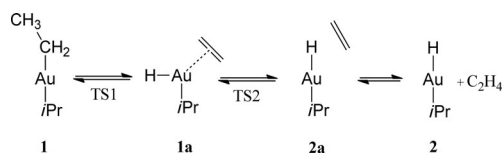
Comparing the B3LYP results to the parameters obtained with the BP86-D3 method, we note in particular the considerable decrease in distance between the (iPr)AuH

and ethene fragments in the van der Waals complex **2a** when dispersion is included. For example, in **2a** the Au...C9 distance shortens by over 0.5 Å from 4.538 to 4.028 Å, and the Au...C12 distance from 5.364 (B3LYP) to 4.819 Å (BP86-D3). This demonstrates the importance of accounting for dispersion when describing such weakly bonded species.

We also notice large discrepancies between some dihedral angles obtained with these methods. For example, for the C10-C18-C21-C48 angle in the gold hydride **2** we obtain a value of 115.6° with B3LYP, and of 90.6° by using BP86-D3, both significantly different from the experimental value of 151.3°. On the other hand, the C2-N3-C10-C18 dihedral in the gold ethyl **1** is calculated as -90.2° (B3LYP) and -80.6° (BP86-D3), compared with the experimental value of -72.9°. Whereas the inclusion of dispersive interactions clearly has a marked influence on the location of the shallow minima of these torsional potentials, it is also evident that this does not always lead to improvement with regard to experiment, presumably because of the complex interplay

of intra- and intermolecular nonbonded interactions that are responsible for their values in the solid state.

The overall reaction scheme for the β -H-elimination in the $(i\text{Pr})\text{AuEt}$ complex according to our calculations is given in Scheme 1, and the associated B3LYP energy profile



Scheme 1. Reaction pathway of the β -H-elimination in $(i\text{Pr})\text{AuEt}$.

in Figure 2. All electronic energies E , ZPE-corrected energies, and free energies G_{298} , as well as energies E_{sol} and G_{sol} calculated with the PCM method with the dielectric constant for the solvent dichloromethane, as well as relative quantities, are listed in Table 2.

Contrary to the situation in alkyl complexes of other transition metals, such as Co ,^[26,27] Rh ,^[26,27] or Cr ,^[28] no isomer displaying an agostic interaction between an alkyl hydrogen and the metal center was found along the reaction path. This is likely a result of gold's filled d-shell in the $(i\text{Pr})\text{AuEt}$ complex, which prevents the formation of a strong 3c–2e bond involving the metal center and the electron pair of the C–H bond that defines an agostic interaction.^[29] Shell-filling also prevents the formation of a π -complex by the donation of olefin π -electrons into empty metal d orbitals, which results in a comparatively high **TS1** barrier between the alkyl structure **1** and the ethene-hydride **1a**, as well as a high relative energy of **1a** compared with **1**. At the B3LYP/cc-pVDZ level of theory the **TS1** electronic energy is 57.1 kcal mol^{−1}, and the ethene-hydride complex **1a** has a relative energy of +34.5 kcal mol^{−1}. This is in sharp contrast with our findings for ethyl complexes of Rh and Co, in which the ethene-hydride complexes are about 10–15 kcal mol^{−1} lower in energy than the α -agostic isomers, and the transition-state energies do not exceed 10 kcal mol^{−1} (see Figure 3 of ref. [21a]). Likewise, in Cr alkyl complexes the ethene-hydride species are only 5 kcal mol^{−1} higher in energy than the α -agostic species, and the maximum transition-state barriers are about 15 kcal mol^{−1} (see Figure 2 of ref. [22]).

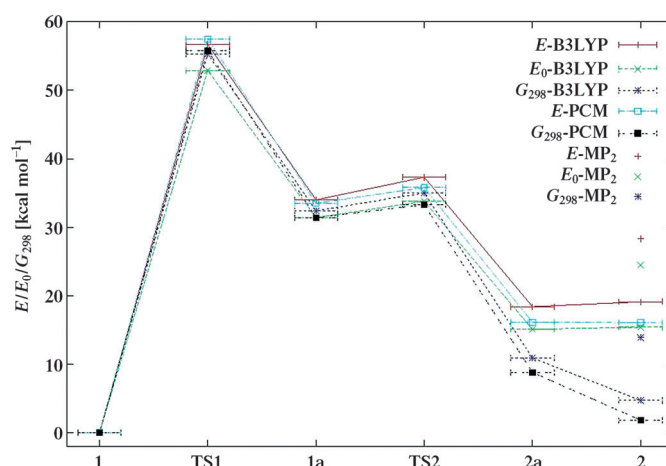


Figure 2. Energy profiles for the thermal decay of $(i\text{Pr})\text{AuEt}$ calculated on the DFT(B3LYP) level of theory. E , E_0 , and G_{298} refer to absolute electronic energies, ZPE-corrected electronic energies, and free energies at 298.15 K, respectively. Results including the effect of the solvent CH_2Cl_2 according to the PCM method as well as relative MP2 energies for $(i\text{Pr})\text{AuEt}$ and $(i\text{Pr})\text{AuH}$ are also displayed. Compound **1** was selected as the isomer of zero energy. Compounds **1**, **1a**, **2a**, and **2** correspond to the ethyl complex, ethene hydride, van der Waals adduct and gold hydride plus free ethene, respectively. **TS1** and **TS2** represent the interconnecting transition states.

Another consequence of the much weaker bonding in **1a** compared with usual transition-metal π -complexes is its easy decay into $(i\text{Pr})\text{AuH}$ and free ethene; according to our calculations this process is exergonic with $\Delta G_{298} = -27.6$ kcal mol^{−1} and a free energy barrier of only 2.5 kcal mol^{−1}. The dissociation of ethene-hydride complexes of Cr, on the

Table 2. Absolute electronic energies E , ZPE-corrected electronic energies E_0 , free energies G_{298} , PCM electronic energies E_{sol} and PCM free energies G_{sol} [Hartree], as well as relative quantities ΔX [kcal mol^{−1}] of stationary points for the thermal decay of $(i\text{Pr})\text{AuEt}$.^[a]

		1	TS1	1a	TS2	2a	2
BP86-D3/def2-SVP	E	−1374.4755	−1374.3901	−1374.4216	−1374.4174	−1374.4390	−1374.4317
	E_0	−1373.8580	−1373.7788	−1373.8080	−1373.8051	−1373.8263	−1373.8201
	G_{298}	−1373.9346	−1373.8553	−1373.8819	−1373.8811	−1373.9060	−1373.9133
	ΔE	0	53.6	33.8	36.5	22.9	27.5
	ΔE_0	0	49.7	31.3	33.2	19.9	23.7
	ΔG_{298}	0	49.7	33.0	33.6	17.9	13.3
	ΔG_{sol}	0	57.1	34.5	37.7	18.8	19.5
B3LYP/cc-pVDZ	E	−1375.1457	−1375.0554	−1375.0914	−1375.0863	−1375.1164	−1375.1152
	E_0	−1374.5140	−1374.4297	−1374.4640	−1374.4602	−1374.4899	−1374.4895
	G_{298}	−1374.5877	−1374.4995	−1374.5361	−1374.5319	−1374.5703	−1374.5802
	E_{sol}	−1375.1559	−1375.0643	−1375.1025	−1375.0918	−1375.1302	−1375.1303
	G_{sol}	−1374.5979	−1374.5085	−1374.5472	−1374.5444	−1374.5841	−1374.5953
	ΔE	0	57.1	34.5	37.7	18.8	19.5
	ΔE_0	0	52.7	31.4	33.9	15.1	15.1
MP2/cc-pVDZ	E	−1370.6814					−1370.6363
	E_0	−1370.0497					−1370.0106
	G_{298}	−1370.1234					−1370.1013
	ΔE	0					28.3
	ΔE_0	0					24.5
	ΔG_{298}	0					13.9
	ΔG_{sol}	0					

[a] Compounds **1**, **1a**, **2a**, and **2** correspond to the ethyl complex, ethene hydride, van der Waals adduct, and gold hydride plus free ethene, respectively. **TS1** and **TS2** represent the interconnecting transition states. Compound **1** was selected as the isomer of zero energy.

other hand, is endergonic by about +5 to 15 kcal mol⁻¹ and has a free energy barrier of about 15 kcal mol⁻¹ (see Figure 5 in ref. [23]), because it corresponds to the energetically unfavorable formation of an empty coordination site in a complex for which the high-spin analogue of the 18 VE rule applies.

The inclusion of the solvent effect does not significantly alter this picture; except for **TS1** the relative electronic energies ΔE and free energies ΔG are lowered in dichloromethane by up to 3.2 kcal mol⁻¹ and are of the same order of magnitude as the ZPE corrections. As a result the G_{sol} values for **1** and **2** become nearly identical, with **1** being only 1.8 kcal mol⁻¹ more stable.

The MP2 calculations agree with the DFT results in predicting **1** to be thermodynamically more stable than the hydride **2**; for the latter we obtain a relative energy/free energy of +28.3/+13.9 kcal mol⁻¹.

Comparing the BP86-D3/def2-SVP reaction energetics with the respective B3LYP/cc-pVDZ values, we note a significant destabilization of **2** relative to **1** with the former method. One may be tempted to regard this solely as a consequence of the loss of dispersion interactions between the gold-hydride complex and the free ethene in **2**. The nearly identical relative energies of **1** and **2** obtained with the BP86-D3 and MP2 methods seem to confirm this interpretation, since the latter also accounts for dispersion interactions. However, a more detailed analysis reveals that this destabilization is partly due to the different functional and partly due to the inclusion of dispersion corrections in BP86-D3.^[30] The same combination of effects leads to a destabilization of the van der Waals complex **2a** relative to **1** by 4–6 kcal mol⁻¹, and a stabilization of **TS1** by 3–5 kcal mol⁻¹.

Kinetics of β -elimination: To assess the significance of the β -H-elimination reaction for Au^I alkyl complexes we used the calculated energies E_0 (BP86-D3/SVP) and thermochemical data to estimate rate constants according to classical transition-state theory (TST).^[31] The TST rate constant k is given by Equation (1):

$$k = \frac{k_B T}{h} \kappa \frac{Q^\ddagger}{Q_r} e^{\frac{\Delta E_0}{k_B T}} \quad (1)$$

in which Q^\ddagger and Q_r are the temperature-dependent partition functions of the transition state and reactant species, and ΔE_0 represents the ZPE-corrected transition-state energy. The transmission coefficient κ was assumed to be unity.

The partition functions are calculated according to the standard expressions for an ideal gas in the canonical ensemble; for details see, for example, ref. [32] and other statistical mechanics texts. The total partition function is obtained as a product of translational, vibrational and rotational contributions, $Q_{\text{Tot}} = Q_{\text{Trans}} \times Q_{\text{Vib}} \times Q_{\text{Rot}}$, which are in turn evaluated in Equations (2)–(4) as follows (by using atomic units):

$$Q_{\text{Trans}} = \left[\frac{M k_B T}{2\pi} \right]^{3/2} V \quad (2)$$

$$Q_{\text{Vib}} = \prod_i \frac{1}{1 - e^{E_i/k_B T}} \quad (3)$$

$$Q_{\text{Rot}} = \frac{(2\pi k_B T)^{3/2} \sqrt{I_A I_B I_C}}{\sigma \pi} \quad (4)$$

in which M and V are the molecular mass and volume for an ideal gas at $p = 0.1$ MPa, respectively, E_i is the energy spacing of the i -th vibrational mode in the harmonic approximation, and I_A , I_B , I_C represent the moments of inertia. The symmetry number σ accounts for the number of rotations in the nuclear permutation group and has been set to unity for all species. The standard scaling factor of 0.9914 for the BP86/SVP method was used for all harmonic frequencies.

Figure 3 summarizes the values of $k(T)$ obtained for the β -H-elimination and its inverse, ethene insertion into the Au–H bond, over the temperature range 350–550 K.

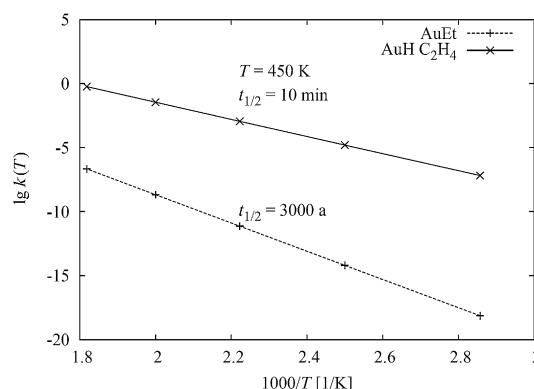


Figure 3. Calculated rate-constants for the thermal decay of (*i*Pr)AuEt (bottom line) and for the insertion of ethene into (*i*Pr)AuH (top line) as a function of temperature. For $T = 450$ K half-lives based on first-order kinetics are given.

It is noted that the high energetic barrier for the β -elimination of the Au^I ethyl complex leads to rather small reaction rates, for example at $T = 450$ K the rate constant for β -elimination becomes $k_{\text{AuEt}} = 7.28 \times 10^{-12} \text{ s}^{-1}$, which corresponds to a half-life of 3000 a assuming first-order kinetics. The experimentally observed decomposition at 180 °C therefore cannot possibly be due to β -elimination.

A quite different picture is obtained for the ethene-insertion reaction, however. The BP86-D3 method leads to a significantly lowered insertion barrier in comparison with our B3LYP results, and the corresponding rate constant and half-life for ethene insertion become $k_{\text{AuH}} = 1.12 \times 10^{-3} \text{ s}^{-1}$ and $\tau_{1/2} = 10$ min, respectively.

Experimental studies: These previous calculations indicated that the *i*PrAu-alkyl complexes rather than being sensitive and unstable compounds should display good thermostabili-

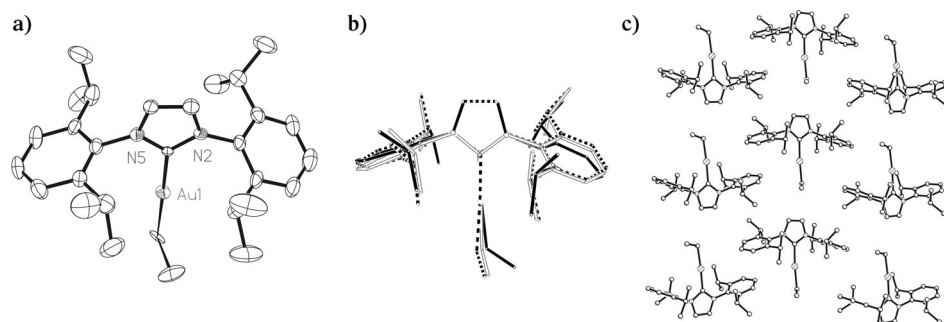


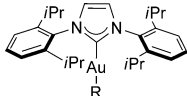
Figure 4. Left: Solid-state molecular structure of **1**. The fitting of the three independent molecules in the elemental cell (middle) shows differences in the orientation of the ligand and the ethyl group. These differences result mainly from the different environment of the three molecules in the crystal. Right: The packing in the crystal lattice.

ties. To verify this prediction from the computational studies, we prepared the *i*Pr-gold(I) complexes **1**, **3**, and **4** bearing different alkyl groups.

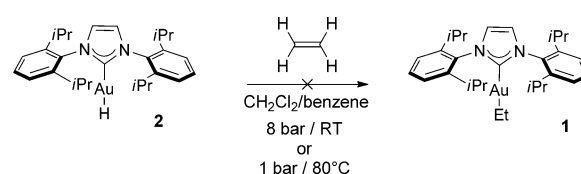
Single crystals of **1** that were suitable for a crystal structure analysis could be grown. The structure is shown in Figure 4^[25].

The results of the thermolysis experiments are shown in Table 3. Unlike the phosphane complexes reported in the literature, all (*i*Pr)Au-alkyl complexes are perfectly stable at 110 °C in toluene, even after 24 h no decomposition could be detected (Table 3, entries 1–3). To switch to higher temperatures, DMSO was used as the solvent; now within 12 h at 180 °C a partial decomposition was detected, but there was no indication that the gold(I) hydride was formed (Table 3, entries 4–6). To re-evaluate the decomposition temperatures of the phosphane alkyl-gold(I) complexes, (Ph)₃PAuEt and (Ph)₃PAuPh were heated to 110 °C in toluene (Table 3, entries 7 and 8). After a short reaction time of 30 min a gold mirror had formed and free (Ph)₃P could be detected by ³¹P NMR spectroscopy.

Table 3. Thermal decomposition of the gold(I) complexes.

 <div style="display: inline-block; vertical-align: middle;"> 1 R = Et 3 R = Me 4 R = Bu </div>		
Compound	Conditions	Result
1 (<i>i</i> Pr)AuMe	[D ₈]Toluene/ 110 °C/24 h	Starting material unchanged
2 (<i>i</i> Pr)AuEt	[D ₈]Toluene/ 110 °C/24 h	Starting material unchanged
3 (<i>i</i> Pr)AuBu	[D ₈]Toluene/ 110 °C/24 h	Starting material unchanged
4 (<i>i</i> Pr)AuMe	[D ₆]DMSO/ 180 °C/12 h	Partial decomposition detectable in the ¹ H NMR spectrum
5 (<i>i</i> Pr)AuEt	[D ₆]DMSO/ 180 °C/12 h	Partial decomposition detectable in the ¹ H NMR spectrum, under these conditions no indication for gold(I) hydride formation
6 (<i>i</i> Pr)AuBu	[D ₆]DMSO/ 180 °C/12 h	Partial decomposition detectable in the ¹ H NMR spectrum, under these conditions no indication for gold(I) hydride formation
7 (Ph) ₃ PAuEt	[D ₈]Toluene/ 110 °C/12 h	After 30 min, formation of a gold mirror. ³¹ P NMR spectrum shows only one peak at δ = −4 ppm corresponding to the free (Ph) ₃ P.
8 (Ph) ₃ PAuPh	[D ₈]Toluene/ 110 °C/12 h	After 30 min, formation of a gold mirror. ³¹ P NMR shows only one peak at δ = −4 ppm corresponding to the free (Ph) ₃ P. Biphenyl formation was detected by GC-MS

Next we turned to the experimental investigation of the reverse reaction (Scheme 2). When (*i*Pr)AuH was subjected to ethene, no conversion to **1** could be detected. This is true for both the experiment at 8 bar of ethene and room temperature and the experiment at 1 bar of ethene at temperatures up to 80 °C. With norbornene, a strained and thus more reactive alkene, up to 50 °C no insertion could be observed either. This differs from the addition of the gold(I) hydride



Scheme 2. No insertion of an unactivated alkene could be observed at 8 bar/RT and at 1 bar/80 °C; compound **1** is not formed.

mentioned in the introduction, which needs an alkyne with two acceptors. On the other hand, the observation is in accordance with the fact that no direct insertion of alkenes and Michael acceptors could be achieved with different organogold(I) compounds, even in stoichiometric reactions.^[33] This also strongly suggests that the previously observed reactions with α,β-unsaturated carbonyl compounds involve an activation of the carbonyl group by gold acting as a Lewis acid rather than an insertion into a gold–carbon bond.^[5b,34]

According to the data from the computational study, for normal alkenes such an insertion should be possible only at temperatures above 150 °C, which is a temperature beyond the decomposition temperature of most known gold catalysts in the presence of organic substrates.

Conclusion

We have carried out a combined experimental and theoretical study on the possibility of β-elimination or alkene insertion in Au^I alkyl or Au^I hydride complexes, respectively.

The barrier height for the β -elimination calculated by using density functional theory clearly rules out the feasibility of this elementary step in catalytic cycles involving gold(I) complexes with NHC ligands. Transition-state theory predicts significant reaction rates for this process only at temperatures above 200 °C. The experimentally observed decomposition of gold(I) alkyl complexes at 180 °C is therefore caused by a different process.

Although considerably lower, the barrier to alkene insertion nevertheless remains significant. The reaction of Au^I hydrides with ethene, for example, should not proceed at temperatures below 100 °C. This theoretical result is also supported by the lack of observing any insertion of even activated alkenes into the gold(I)-hydride bond at moderate temperatures.

We believe the increased barrier height for the β -elimination/migratory-insertion reaction, as well as the decreased relative stability of the gold(I) olefin hydride compared with other early and late transition metals, to be a consequence of the filled d-shell of gold(I). This also results in a conspicuous absence of agostic interactions in Au^I alkyl complexes, which are near-ubiquitous in early as well as late transition-metal complexes of higher alkyls.

Complexes of gold in higher oxidation-states are expected to behave differently, because empty d orbitals may become available for bonding.

Experimental Section

Material and methods: All reagents were used without further purification unless otherwise noted. Dry solvents were dispensed from solvent purification system MB SPS-800. The preparation of air- and moisture-sensitive materials was carried out in flame dried flasks under an atmosphere of dinitrogen using Schlenk-techniques. Reactions were performed in dry and degassed solvents. Thin-layer chromatography (TLC) was performed using Polygram pre-coated plastic sheets SIL G/UV254 (SiO₂, 0.20 mm) and Alugram pre-coated aluminium sheets SIL G/UV254 (SiO₂, 0.20 mm) from Macherey–Nagel. Column chromatography was performed by using silica gel (40.0–63.0 nm particle size) from Macherey–Nagel. NMR spectra were recorded on Bruker Avance 500, Bruker Avance 300 and Bruker ARX-250 spectrometers at RT. Chemical shifts (in ppm) were referenced to residual solvent proton/carbon peak or using external standard 85 % H₃PO₄ for ³¹P NMR spectroscopy. Signal multiplicity was determined as s (singlet), d (doublet), t (triplet), q (quartet) or m (multiplet). ¹³C assignment was achieved DEPT135 spectra. MS spectra were recorded on a Vakkum Generators ZAB-2F, Finnigan MAT TSQ 700 or a JEOL JMS-700 spectrometer. GC-MS spectra were recorded on an Agilent 5890 Series II Plus with a HP 5972 mass analyzer. IR spectra were recorded on a Bruker Vector 22 FT-IR. Crystal structure analysis was accomplished on Bruker Smart CCD or Bruker APEX diffractometers.

Procedure A: iPrAuCl (200 mg, 1 equiv) was dissolved in THF (0.04 M) in a flame-dried Schlenk flask in an atmosphere of dinitrogen and cooled to –20 °C. The Grignard reagent (4 equiv) was added slowly. The mixture was allowed to warm to RT and stirred for 3 h. The reaction mixture was then quenched with 2–3 drops of water and stirred for 10 min, then dried over Na₂SO₄, filtered through a plug of Celite, topped by a layer of neutral aluminium oxide. The solution was concentrated in vacuo to afford the gold complex.

Procedure B: iPrAuCl (1 equiv) was dissolved in THF (0.04 M) in a flame-dried Schlenk flask in an atmosphere of dinitrogen and cooled to

–78 °C. The organolithium reagent (4 equiv) was added slowly. The mixture was allowed to warm to RT and stirred for 3 h. The reaction mixture was then quenched with 2–3 drops of water and stirred for 10 min, then dried over Na₂SO₄, filtered through a plug of Celite, topped by a layer of neutral aluminium oxide. The solution was concentrated in vacuo to afford the gold complex.

(Ph₃P)AuEt and (Ph₃P)AuPh were prepared according to the literature procedure.^[33]

{1,3-bis[2,6-bis(1-methylethyl)phenyl]-1,3-dihydro-2H-imidazol-2-ylidene(ethyl)gold (1): Compound **1** was prepared according to procedure A on a 0.322 mmol scale in 95 % yield.^[35] ¹H NMR (301 MHz, CD₂Cl₂): δ = 7.52 (t, J = 7.5 Hz, 2H), 7.30–7.37 (m, 4H), 7.10 (s, 2H), 2.64 (sept, J = 6.9 Hz, 4H), 1.35 (d, J = 6.9 Hz, 12H), 1.22 (d, J = 6.9 Hz, 12H), 0.86 (t, J = 7.9 Hz, 3H), 0.54 ppm (q, J = 7.9 Hz, 2H); ¹H NMR (301 MHz, DMSO): δ = 0.35 (q, J = 7.9 Hz, 2H), 0.76 (t, J = 7.9 Hz, 3H), 1.18 (d, J = 6.9 Hz, 12H), 1.27 (d, J = 6.8 Hz, 12H), 2.57 (sept, J = 6.8 Hz, 4H), 7.35 (d, J = 7.7 Hz, 4H), 7.50–7.55 (m, 2H), 7.72 ppm (s, 2H); ¹³C NMR (126 MHz, CD₂Cl₂): δ = 13.0, 16.8, 24.0 (4C), 24.5 (4C), 29.1 (4C), 123.0 (2C), 124.2 (4C), 130.3 (2C), 135.4 (2C), 146.4 (4C), 201.9 ppm; IR (Film): $\tilde{\nu}$ = 3163, 3137, 3074, 2965, 2869, 3803, 2301, 2196, 1678, 1593, 1552, 1472, 1413, 1385, 1256, 1214, 1181, 1106, 1059, 992, 954, 711, 676, 532, 451 cm^{–1}.

{1,3-bis[2,6-bis(1-methylethyl)phenyl]-1,3-dihydro-2H-imidazol-2-ylidene(hydride)gold (2): Compound **2** was prepared according to the literature procedure.^[6a] ¹H NMR (301 MHz, CD₂Cl₂): δ = 1.22 (d, J = 6.9 Hz, 6H), 1.34 (d, J = 6.9 Hz, 6H), 2.60 (sept, J = 6.8 Hz, 2H), 3.39 (s, 1H), 7.16 (s, 2H), 7.30–7.37 (m, 4H), 7.54 ppm (t, J = 7.2 Hz, 2H). ¹H NMR spectroscopy data matched with that reported previously.^[6a]

{1,3-bis[2,6-bis(1-methylethyl)phenyl]-1,3-dihydro-2H-imidazol-2-ylidene(methyl)gold (3): Compound **3** was prepared according to procedure A on 0.161 mmol scale in 83 % yield.^[36] ¹H NMR (301 MHz, CD₂Cl₂): δ = –0.28 (s, 3H), 1.22 (d, J = 6.9 Hz, 12H), 1.35 (d, J = 6.8 Hz, 12H), 2.65 (sept, J = 6.9 Hz, 4H), 7.11 (s, 2H), 7.33 (d, J = 7.7 Hz, 4H), 7.53 ppm (t, J = 7.8 Hz, 2H); ¹H NMR (500 MHz, DMSO): δ = –0.46 (s, 3H), 1.18 (d, J = 6.9 Hz, 12H), 1.28 (d, J = 6.9 Hz, 12H), 2.58 (sept, J = 6.8 Hz, 4H), 7.36 (d, J = 7.8 Hz, 2H), 7.50–7.54 (m, 2H), 7.79 ppm (s, 2H).

{1,3-bis[2,6-bis(1-methylethyl)phenyl]-1,3-dihydro-2H-imidazol-2-ylidene(butyl)gold (4): Compound **4** was prepared according to procedure B on a 0.161 mmol scale in 88 % yield. ¹H NMR (400 MHz, CD₂Cl₂): δ = 0.59 (t, J = 7.3 Hz, 3H), 0.66 (t, J = 7.3 Hz, 2H), 0.85 (qu, J = 7.4 Hz, 2H), 1.21 (d, J = 6.9 Hz, 12H), 1.28 (qu, J = 7.4 Hz, 2H), 1.35 (d, J = 6.9 Hz, 12H), 2.64 (sept, J = 6.8 Hz, 4H), 7.11 (s, 2H), 7.31 (d, J = 7.8 Hz, 4H), 7.51 (t, J = 7.8 Hz, 2H); ¹H NMR (301 MHz, DMSO): δ = 0.43–0.59 (m, 5H), 0.80 (t, J = 7.3 Hz, 2H), 1.20 (d, J = 6.9 Hz, 12H), 1.25 (m, 2H), 1.29 (d, J = 6.8 Hz, 12H), 2.57 (sept, J = 6.8 Hz, 4H), 7.36 (d, J = 7.7 Hz, 4H), 7.49–7.55 ppm (m, 2H), 7.73 ppm (s, 2H); ¹³C NMR (101 MHz, CD₂Cl₂): δ = 14.2, 21.5, 24.1 (4C), 24.4 (4C), 29.0, 29.1 (4C), 34.9, 122.9 (2C), 124.2 (4C), 130.3 (2C), 135.4 (2C), 146.4 (4C), 202.6; IR (KBr): $\tilde{\nu}$ = 3161, 2963, 2926, 2868, 2790, 2303, 2197, 1471, 1412, 1384, 1365, 1342, 1106, 1058955, 803, 756, 711, 548, 449 cm^{–1}; MS (FAB⁺): m/z : 641 [M–H]⁺; HRMS (FAB⁺): calcd for C₃₁H₄₄AuN₂: 641.3170 [C₃₁H₄₄AuN₂]⁺; found 641.3190.

Thermolysis experiments: The gold complex (24.0 μ mol) was dissolved in deuterated toluene (600 μ L) or deuterated DMSO (600 μ L) in a NMR tube and heated to 110 °C for 24 h or 180 °C for 12 h, respectively.

Insertion experiments: a) In a flame-dried Schlenk flask under an atmosphere of ethene, the gold hydride complex (51.0 μ mol) was dissolved in deuterated benzene. A stream of ethene was bubbled through the reaction mixture for 30 min. Then the reaction was heated to 80 °C for 12 h.

b) In a pressure-resistant NMR tube the gold complex was dissolved in deuterated dichloromethane under a pressure of 8 bar of ethene for 24 h.

Acknowledgements

This work was supported by the Deutsche Forschungsgemeinschaft through Sonderforschungsbereich 623 “Molekulare Katalysatoren: Struktur und Funktionsdesign”. The authors wish to express their gratitude to Mikko Muuronen for very helpful advice and assistance concerning the DFT-D3 calculations.

- [1] a) X. Wang, L. Andrews, *J. Am. Chem. Soc.* **2001**, *123*, 12899–12900; b) X. Wang, L. Andrews, *Angew. Chem.* **2003**, *115*, 5359–5364; *Angew. Chem. Int. Ed.* **2003**, *42*, 5201–5206; c) L. Andrews, X. Wang, *J. Am. Chem. Soc.* **2003**, *125*, 11751–11760; for a detailed discussion, see: d) M.-J. Crawford, T. M. Klapötke, *Angew. Chem.* **2002**, *114*, 2373–2375; *Angew. Chem. Int. Ed.* **2002**, *41*, 2269–2271.
- [2] a) A. S. K. Hashmi, G. J. Hutchings, *Angew. Chem.* **2006**, *118*, 8064–8105; *Angew. Chem. Int. Ed.* **2006**, *45*, 7896–7936; b) A. Fürstner, P. W. Davis, *Angew. Chem.* **2007**, *119*, 3478–3519; *Angew. Chem. Int. Ed.* **2007**, *46*, 3410–3449; c) A. S. K. Hashmi, *Chem. Rev.* **2007**, *107*, 3180–3211; d) A. Arcadi, *Chem. Rev.* **2008**, *108*, 3266–3325; e) E. Jiménez-Núñez, A. M. Echavarren, *Chem. Rev.* **2008**, *108*, 3326–3350; f) Z. G. Li, C. Brouwer, C. He, *Chem. Rev.* **2008**, *108*, 3239–3265; g) D. J. Gorin, B. D. Sherry, F. D. Toste, *Chem. Rev.* **2008**, *108*, 3351–3378; h) A. S. K. Hashmi, M. Bührle, *Aldrichimica Acta* **2010**, *43*, 27–33.
- [3] For a detailed study of the thermal decomposition of alkyl-gold(I) complexes, see: A. Tamaki, J. K. Kochi, *J. Organomet. Chem.* **1973**, *61*, 441–450.
- [4] a) H. H. Brintzinger, D. Fischer, R. Mülhaupt, B. Rieger, R. M. Waymouth, *Angew. Chem.* **1995**, *107*, 1255–1283; *Angew. Chem. Int. Ed. Engl.* **1995**, *34*, 1143–1170; b) M. Delferro, T. J. Marks, *Chem. Rev.* **2011**, *111*, 2450–2485.
- [5] a) R. T. Baker, P. Nguyen, T. B. Marder, S. A. Westcott, *Angew. Chem.* **1995**, *107*, 1451–1452; *Angew. Chem. Int. Ed. Engl.* **1995**, *34*, 1336–1338; b) A. S. K. Hashmi, L. Schwarz, J.-H. Choi, T. M. Frost, *Angew. Chem.* **2000**, *112*, 2382–2385; *Angew. Chem. Int. Ed.* **2000**, *39*, 2285–2288.
- [6] a) E. Y. Tsui, P. Müller, J. P. Sadighi, *Angew. Chem.* **2008**, *120*, 9069–9072; *Angew. Chem. Int. Ed.* **2008**, *47*, 8937–8940; before, gold(I) hydride had only been detected in the gas phase: b) U. Ringström, *Nature* **1963**, *198*, 981.
- [7] a) A. L. Escalle, G. Mora, F. Gagosz, N. Mézailles, X. F. Le Goff, Y. Jean, P. Le Floch, *Inorg. Chem.* **2009**, *48*, 8415–8422; for the previous description of mixed-metal dinuclear gold hydrides with bridging hydrides, see: H. Lehner, D. Matt, P. S. Pregosin, L. M. Venanzi, A. Albinati, *J. Am. Chem. Soc.* **1982**, *104*, 6825–6827.
- [8] A. Comas-Vives, C. González-Arellano, A. Corma, M. Iglesias, F. Sánchez, G. Ujaque, *J. Am. Chem. Soc.* **2006**, *128*, 4756–4765.
- [9] H. Ito, K. Takagi, T. Miyahara, M. Sawamura, *Org. Lett.* **2005**, *7*, 3001–3004.
- [10] H. Ito, T. Saito, T. Miyahara, C. Zhong, M. Sawamura, *Organometallics* **2009**, *28*, 4829–4840.
- [11] B. Alcaide, P. Almendros, T. M. del Campo, I. Fernandez, *Chem. Commun.* **2011**, *47*, 9054–9056.
- [12] Gaussian 09, Revision B.01, M. J. Frisch, G. W. Trucks, H. B. Schlegel, G. E. Scuseria, M. A. Robb, J. R. Cheeseman, G. Scalmani, V. Barone, B. Mennucci, G. A. Petersson, H. Nakatsuji, M. Caricato, X. Li, H. P. Hratchian, A. F. Izmaylov, J. Bloino, G. Zheng, J. L. Sonnenberg, M. Hada, M. Ehara, K. Toyota, R. Fukuda, J. Hasegawa, M. Ishida, T. Nakajima, Y. Honda, O. Kitao, H. Nakai, T. Vreven, J. A. Montgomery, Jr., J. E. Peralta, F. Ogliaro, M. Bearpark, J. J. Heyd, E. Brothers, K. N. Kudin, V. N. Staroverov, T. Keith, R. Kobayashi, J. Normand, K. Raghavachari, A. Rendell, J. C. Burant, S. S. Iyengar, J. Tomasi, M. Cossi, N. Rega, J. M. Millam, M. Klene, J. E. Knox, J. B. Cross, V. Bakken, C. Adamo, J. Jaramillo, R. Gomperts, R. E. Stratmann, O. Yazyev, A. J. Austin, R. Cammi, C. Pomelli, J. W. Ochterski, R. L. Martin, K. Morokuma, V. G. Zakrzewski, G. A. Voth, P. Salvador, J. J. Dannenberg, S. Dapprich, A. D. Daniels, O. Farkas, J. B. Foresman, J. V. Ortiz, J. Cioslowski, D. J. Fox, Gaussian, Inc., Wallingford CT, **2010**.
- [13] K. A. Peterson, C. Pizzarini, *Theor. Chem. Acc.* **2005**, *114*, 283–296.
- [14] T. H. Dunning, *J. Chem. Phys.* **1989**, *90*, 1007–1023.
- [15] D. Figgen, G. Rauhut, M. Dolg, H. Stoll, *Chem. Phys.* **2005**, *311*, 227–244.
- [16] S. Niu, M. B. Hall, *Chem. Rev.* **2000**, *100*, 353–405.
- [17] T. A. Halgren, W. N. Lipscomb, *Chem. Phys. Lett.* **1977**, *49*, 225–232.
- [18] C. Peng, H. B. Schlegel, *Isr. J. Chem.* **1993**, *33*, 449–454.
- [19] S. Grimme, J. Antony, S. Ehrlich, H. Krieg, *J. Chem. Phys.* **2010**, *132*, 154104.
- [20] TURBOMOLE V6.4 2012, a development of University of Karlsruhe and Forschungszentrum Karlsruhe GmbH, 1989–2007; TURBOMOLE GmbH, since 2007; available from <http://www.turbomole.com>.
- [21] M. Muuronen, J. E. Perea-Buceta, M. Nieger, M. Patzschke, J. Helaja, *Organometallics* **2012**, *31*, 4320–4330.
- [22] a) A. Schäfer, C. Huber, R. Ahlrichs, *J. Chem. Phys.* **1994**, *100*, 5829–5835; b) F. Weigend, M. Häser, H. Patzelt, R. Ahlrichs, *Chem. Phys. Lett.* **1998**, *294*, 143–152; c) F. Weigend, R. Ahlrichs, *Phys. Chem. Chem. Phys.* **2005**, *7*, 3297–3305.
- [23] a) M. Sierka, A. Hogeckamp, R. Ahlrichs, *J. Chem. Phys.* **2003**, *118*, 9136–9148; b) K. Eichkorn, F. Weigend, O. Treutler, R. Ahlrichs, *Theor. Chem. Acc.* **1997**, *97*, 119–124; c) F. Weigend, *Phys. Chem. Chem. Phys.* **2006**, *8*, 1057–1065; d) A. Hellweg, C. Hättig, S. Höfener, W. Klopper, *Theor. Chem. Acc.* **2007**, *117*, 587–597.
- [24] D. Andrae, U. Haeussermann, M. Dolg, H. Stoll, H. Preuss, *Theor. Chim. Acta* **1990**, *77*, 123.
- [25] CCDC-897806 (1) contains the supplementary crystallographic data for this paper. These data can be obtained free of charge from The Cambridge Crystallographic Data Centre via www.ccdc.cam.ac.uk/data_request/cif.
- [26] R. Xu, G. Klatt, H. Wadeh, H. Köppel, *Inorg. Chem.* **2010**, *49*, 3289–3296.
- [27] R. Xu, M. Bittner, G. Klatt, H. Köppel, *J. Phys. Chem. A* **2008**, *112*, 13139–13148.
- [28] R. Xu, G. Klatt, M. Enders, H. Köppel, *J. Phys. Chem. A* **2012**, *116*, 1077–1085.
- [29] For a recent review of theoretical aspects of the agostic interaction, see: E. Clot, O. Eisenstein, *Struct. Bonding* **2004**, *113*, 1–36.
- [30] G. Klatt, unpublished results.
- [31] For modern discussions of transition-state theory, see: a) P. Pechukas, in *Dynamics of Molecular Collisions*, Part B, (Ed.: W. H. Miller), Plenum, New York, **1976**; Chapter 6; b) W. H. Miller, *Acc. Chem. Res.* **1976**, *9*, 306–312; c) D. G. Truhlar, W. L. Hase, J. T. Hynes, *J. Phys. Chem.* **1983**, *87*, 2664–2682.
- [32] D. A. McQuarrie, *Statistical Thermodynamics*, Harper & Row, New York, **1976**.
- [33] A. S. K. Hashmi, T. D. Ramamurthi, F. Rominger, *J. Organomet. Chem.* **2009**, *694*, 592–597.
- [34] a) G. Dyker, E. Muth, A. S. K. Hashmi, L. Ding, *Adv. Synth. Catal.* **2003**, *345*, 1247–1252; b) A. S. K. Hashmi, L. Schwarz, P. Rubenbauer, M. C. Blanco, *Adv. Synth. Catal.* **2006**, *348*, 705–708.
- [35] V. J. Scott, J. A. Labinger, J. E. Bercaw, *Organometallics* **2010**, *29*, 4090–4096.
- [36] N. P. Mankad, F. D. Toste, *J. Am. Chem. Soc.* **2010**, *132*, 12859–12861.

Received: August 27, 2012

Revised: December 10, 2012

Published online: February 10, 2013